



**Structural and biochemical analyses of glycoside
hydrolase families 5 and 26 β -(1,4)-mannanases from
Podospira anserina reveal differences upon
manno-oligosaccharide catalysis**

Marie Couturier, Alain Roussel, Anna Rosengren, Philippe Leone, Henrik
Stålbrand, Jean-Guy Berrin

► **To cite this version:**

Marie Couturier, Alain Roussel, Anna Rosengren, Philippe Leone, Henrik Stålbrand, et al.. Structural and biochemical analyses of glycoside hydrolase families 5 and 26 β -(1,4)-mannanases from Podospira anserina reveal differences upon manno-oligosaccharide catalysis. Journal of Biological Chemistry, 2013, 288 (20), pp.14624-14635. 10.1074/jbc.M113.459438 . hal-01268087

HAL Id: hal-01268087

<https://hal.science/hal-01268087>

Submitted on 29 May 2020

HAL is a multi-disciplinary open access archive for the deposit and dissemination of scientific research documents, whether they are published or not. The documents may come from teaching and research institutions in France or abroad, or from public or private research centers.

L'archive ouverte pluridisciplinaire **HAL**, est destinée au dépôt et à la diffusion de documents scientifiques de niveau recherche, publiés ou non, émanant des établissements d'enseignement et de recherche français ou étrangers, des laboratoires publics ou privés.

Structural and biochemical analyses of glycoside hydrolase families 5 and 26 β -(1,4)-mannanases from *Podospora anserina* reveal differences upon manno-oligosaccharides catalysis*

Marie Couturier¹, Alain Roussel², Anna Rosengren³, Philippe Leone², Henrik Stålbrand³, and Jean-Guy Berrin¹

¹INRA, UMR1163 BCF, Aix Marseille Université, Polytech Marseille, F-13288 Marseille, France

²Architecture et Fonction des Macromolécules Biologiques, Aix Marseille Université, CNRS UMR7257, F-13288 Marseille, France

³Department of Biochemistry and Structural Biology, Lund University, P.O. Box 124, S-221 00, Lund, Sweden

*Running title : *Structural and biochemical characterization of two P. anserina mannanases*

To whom correspondence should be addressed: Jean-Guy Berrin, INRA, Laboratoire de Biotechnologie des Champignons Filamenteux, Marseille, France. Tel: +33(0)4 91 82 86 04; Fax: +33(0)4 91 82 86 01; E-mail: jean-guy.berrin@univ-amu.fr

Keywords: Mannanases, Glycoside hydrolase, CAZy, *Podospora anserina*, 3D structure, GH5, GH26, CBM35

Background: Fungal mannanases contribute to enzymatic degradation of lignocellulose.

Results: New fungal mannanases reveal striking differences in substrate specificities. A rigid linker tightly connects the family 26 glycoside hydrolase to its binding module.

Conclusion: *Podospora anserina* mannanases display differences in substrate binding modes, transglycosylation activity and modular organization.

Significance: Information on the structure-function relationships of fungal mannanases is essential to improve the comprehension of biomass deconstruction.

SUMMARY

The microbial deconstruction of the plant cell wall is a key biological process that is of increasing importance with the development of a sustainable biofuel industry. The glycoside hydrolase families GH5 (*PaMan5A*) and GH26 (*PaMan26A*) endo- β -1,4-mannanases from the coprophilic ascomycete *Podospora anserina* contribute to the enzymatic degradation of lignocellulosic biomass. In this study, *P. anserina* mannanases were further subjected to detailed comparative analysis of their substrate specificities, active site organization and transglycosylation capacity. Although *PaMan5A* displays a classical mode of action, *PaMan26A* revealed

an atypical hydrolysis pattern with the release of mannotetraose and mannose from mannopentaose resulting from a predominant binding mode involving the -4 subsite. The crystal structures of *PaMan5A* and *PaMan26A* were solved at 1.4Å and 2.85Å resolution, respectively. Analysis of the *PaMan26A* structure supported strong interaction with substrate at the -4 subsite mediated by two aromatic residues W244 and W245. The *PaMan26A* structure appended to its family 35 carbohydrate-binding module revealed a short and proline-rich rigid linker that anchored together the catalytic and the binding modules.

Endo- β -1,4 mannanases (β -mannanases, E.C. 3.2.1.78) catalyse the random hydrolysis of manno-glycosidic bonds in mannans and heteromannans. These polysaccharides are the main components of hemicellulose in softwoods and are found in smaller amounts in angiosperms (1). Mannans comprise a backbone of β -1,4-linked D-mannose residues, known as mannan, or a heterogeneous combination of β -1,4-D-mannose and β -1,4-D-glucose units, termed glucomannan. Both can be decorated with α -1,6-linked galactose side chains and these polysaccharides are referred to as galactomannan and galactoglucomannan, respectively.

Several types of glycoside hydrolases⁴ (GH) are required for complete degradation of mannans and endo- β -1,4 mannanases are the key enzymes. In the CAZy database (www.cazy.org; (2)), β -1,4 mannanase activities are found in families GH5, GH26 and GH113. The three families belong to clan GH-A; they share the same (β/α)₈-barrel protein fold, catalytic machinery and retaining double displacement mechanism (3,4,5). Because of this retaining double displacement mechanism, some of these enzymes are able to perform transglycosylation, in which a carbohydrate hydroxyl group can act as an acceptor molecule rather than water as is the case in hydrolysis. Transglycosylation thus leads to the synthesis of new glycosides or oligosaccharides longer than the original substrate. GH5 and GH113 mannanases have been described as able to catalyse transglycosylation reactions (6,7,8,9), while to date no evidence of transglycosylation has been reported for GH26 mannanases (10). β -mannanases are frequently encountered as modular enzymes. Indeed, some harbor CBM from families CBM1, CBM6, CBM10, CBM31, CBM35 (11,12). It is generally observed that the linker regions between catalytic module and CBM display a great deal of structural flexibility to maximize substrate accessibility, as it has been confirmed by the few crystal structures of bacterial modular enzymes (13,14).

GH5 endo- β -1,4 mannanases, which are found in bacteria, fungi, animals and plants are the most largely characterized family. To date only three eukaryotic endo-mannanase 3D structures from family GH5 are available: one from *Trichoderma reesei* (PDB 1QNO; (15)), one from the blue mussel *Mytilus edulis* (PDB 2C0H; (7)) and one from the tomato fruit *Solanum lycopersicum* (PDB 1RH9; (16)). Although several family GH26 endo- β -1,4 mannanases have also been characterized from different organisms (e.g., *Cellulomonas fimi* (17), *Cellvibrio japonicus* (18), *Pyromyces equi* (19)), only sparse studies have focused on GH26 endo- β -1,4-mannanases of fungal origin and the five 3D structures available (*B. subtilis*, PDB 2WHK, (20); *Bacillus subtilis* PDB 2QHA, (21); *C. fimi* PDB 2BVT, (17); *C. japonicus* PDB 1GVY (22) and PDB 2VX4 (23)) are all from bacteria and represent only catalytic domains (CDs).

The characterization of endo- β -1,4 mannanases biochemical properties and substrate

specificities revealed that many release essentially mannobiose and mannotriose as end products (9, 17, 24, 25), and that their active site display generally 5 to 6 subsites able to accommodate the substrate (10,15). Although GH5 and GH26 mannanases share some characteristics, several studies revealed different modes of action. In particular, biochemical studies pointed to divergence in specificity between GH5 and GH26 bacterial mannanases, suggesting different biological role (20, 26).

The coprophilic fungus *Podospora anserina* has one of the largest fungal set of candidate enzymes for cellulose and hemicellulose degradation described to date and one of the highest numbers of carbohydrate-binding modules (CBMs) of all the fungal genomes available (27). In a previous study, comparative genomics was used which identified two mannanases from families GH5 (*PaMan5A*) and GH26 (*PaMan26A*) in the *Podospora anserina* genome (28). Investigation of the contribution made by each *P. anserina* mannanase to the saccharification of spruce demonstrated that they individually supplemented the secretome of the industrial *T. reesei* CL847 strain. The most striking effect was obtained with *PaMan5A* that improved the release of total sugars by 28% and of glucose by 18% (28). In the present study, *P. anserina* GH5 and GH26 mannanases were subjected to detailed comparative analysis of their substrate specificities, active site organisation and transglycosylation capacity. The three-dimensional structures of *PaMan5A* and *PaMan26A* linked to a CBM35 module were solved in their native form at 1.4Å and 2.85Å resolution, respectively.

EXPERIMENTAL PROCEDURES

Production and purification of PaMan5A and PaMan26A

PaMan5A and *PaMan26A* were produced in *P. pastoris* 2 liters cultures and purified as described previously in (28). Enzyme purification was completed by an additional size exclusion chromatographic step. After the nickel chelate purification step, the eluate containing *PaMan5A* or *PaMan26A* was concentrated using a Vivaspin with 10-kDa cut-off polyethersulfone membrane, (Sartorius, Palaiseau, France) and dialysed against the buffer used for the size exclusion chromatography (Hepes 20 mM pH 7.5, NaCl

150 mM). The concentrated fraction was subsequently loaded onto a Superdex S200 HiLoad 16/60 column (Amersham, Buckinghamshire, UK). The fractions containing *PaMan5A* or *PaMan26A* were pooled and concentrated as described above.

Construction of site-specific variants

Site-directed mutagenesis was performed using Quickchange kit (Stratagene), with primers listed in Table 1, according to the instructions of manufacturer. Using the wild-type *PaMan5A* and *PaMan26A* plasmids described in (28), active-site variants were designed for each enzyme. Two single-site mutants were constructed for each enzyme: E177A and E283A for *PaMan5A* and E300A and E390A for *PaMan26A*.

Transformation was performed in *P. pastoris* and production and purification of enzyme variants were carried out as described above.

Deglycosylation assay

N-glycosylation sites were predicted using the NetNGlyc 1.0 Server (<http://www.cbs.dtu.dk/services/NetNGlyc/>).

To remove N-linked glycans, purified enzymes were treated with PNGase F (NEB, Ipswich, MA, USA) under denaturing conditions according to manufacturer's instructions. Briefly, 10 µg of protein were incubated in 0.5% SDS and 40 mM DTT and boiled for 10 minutes for complete denaturation. Denatured samples were subsequently incubated with 1,500 units of PNGase F in appropriate buffer for one hour at 37°C. Deglycosylated and control samples were analysed by SDS-PAGE (BioRad, Marnes-la-Coquette, France).

Analysis of end products release from polysaccharides

The activity of *PaMan5A* and *PaMan26A* was assayed towards glucomannan, galactomannan and linear mannan. Briefly, a 1% w/v solution was prepared in 50 mM Na-acetate buffer, pH 5.2. The assay was performed by incubating 75 µg of enzyme with 90 µl of 1% w/v substrate solution or suspension at 40°C for 30 minutes. After hydrolysis, mono- and oligo-saccharides were analyzed using high performance anion exchange chromatography (HPAEC) coupled with pulsed amperometric detection (PAD) (ICS 3000; Dionex, Sunnyvale, USA) equipped with a carbo-Pac PA-1 analytical column (250 × 4 mm). 10 µl samples of enzymatic reactions

were stopped by the addition of 90 µl of 100 mM NaOH before injection (5 µl) into the HPAEC system. Elution was carried out in 130 mM NaOH using a 25-min linear gradient program from 100% A (130 mM NaOH) to 60% A and 40% B (NaOAc, 500 mM; NaOH, 130 mM). All the assays were carried out in triplicate.

Hydrolysis product formation from oligosaccharides and determination of kinetic parameters

Products generated after hydrolysis of manno-oligosaccharides were analysed using HPAEC-PAD as described above. 20 µl of suitably diluted enzyme were incubated at 40°C for various time lengths with 180 µl of 100 µM substrate in 50 mM acetate buffer pH 5.2. Calibration curves were plotted using β-1,4-manno-oligosaccharides as standards from which response factors were calculated (Chromeleon program, Dionex) and used to determine the amount of products released at different time points. All the assays were carried out in duplicates. The data were fitted to the equation of Matsui (29, 30), $k = \ln[S_0]/[S_t]$, where $k = (k_{cat}/K_m)[\text{enzyme}] \times \text{time}$ and $[S_0]$ and $[S_t]$ represent substrate concentration prior to the start of the reaction and at a specified time during the reaction, respectively.

Hydrolysis of M_5 and M_6 in $H_2^{18}O$

To determine and compare the hydrolytic cleavage patterns of M_5 and M_6 by *PaMan5A* and *PaMan26A*, HPAEC-PAD data on the hydrolysis products (as described above) was combined with the analysis of hydrolysis performed in $H_2^{18}O$ as described previously (31, 32). Each productive binding of M_5 or M_6 gives rise to two products (e.g. M_6 cleaved to either two molecules of M_3 or to M_5 and M_1 or to M_4 and M_2). Quantitative HPAEC-PAD analysis of one product per cleavage (M_3 , M_4 and M_5 , respectively) was used to calculate the relative frequency of the productive binding modes of M_5 and M_6 that give rise to these products. Each of these products can further be produced by either of two binding modes and to distinguish between these two modes, the ratio of non-labeled (^{16}O) and labeled (^{18}O) product (M_3 , M_4 and M_5) was used. Reactions were performed at 8°C (low temperature was used to avoid spontaneous incorporation of ^{18}O , (31)) in $H_2^{18}O$ (93%, with a total of 7% $H_2^{16}O$ contamination (3% in the original $H_2^{18}O$ and

4% from the enzyme and substrate stock solutions) containing 1 mM Na-acetate buffer pH 5, 0.8 mM substrate, and 0.1 μ M enzyme. Samples (0.5 μ l) were withdrawn at different time points (0-60 min) and spotted directly on a stainless steel plate for Matrix-Assisted Laser Desorption Ionization-Time-of-Flight Mass Spectrometry (MALDI-TOF MS) analysis. Matrix (DHB 10 mg.ml⁻¹ in H₂O) was applied immediately to the sample and it was dried under warm air. Samples from 40 min and 60 min had sufficient product build up and the determined ratios were in good agreement (2-8% variation between the 40 min and the 60 min samples from each incubation). The data from 40 min samples was used.

MALDI-TOF MS data acquisition and analysis

MALDI-TOF MS spectra were recorded in positive reflector mode using a 4700 Proteomics Analyzer (Applied Biosystems, Framingham, MA, USA). The laser intensity was set at 5500, and 50 subspectra with 20 shots on each were accumulated from each sample spot. The program Data Explorer version 4.5 was used for analysis of the data. The relative frequencies of the different productive binding modes resulting in the same products were calculated from the relative areas of the monoisotopic peaks of ¹⁶O- and ¹⁸O-labeled products as previously described (31). Two corrections were made: one for the [M + 2] natural isotope peak (5.3 % of the monoisotopic peak for M₃, 8 % of the monoisotopic peak for M₄ and 11 % of the monoisotopic peak for M₅) of the light (¹⁶O) species that overlaps with the heavy (¹⁸O) peak, followed by another correction for the 7 % H₂¹⁶O contamination in the hydrolysis assays. M₁ was not detectable because of matrix suppression of low masses.

Transglycosylation analysis

Reactions were set up to aim for detection of transglycosylation products with MALDI-TOF-MS, similarly to what was done in (32). Five mM M₅ was incubated with 0.5 μ M PaMan5A at 40°C in 10 mM Na-acetate buffer pH 5 for 0-15 min. Samples (0.5 μ l) were withdrawn at different time points and spotted directly onto a stainless steel MALDI plate. Matrix solution (DHB 10 mg.ml⁻¹ in water) was applied (0.5 μ l) and the samples were dried under warm air.

Data acquisition and analysis was performed as described above.

Protein crystallization, data collection and processing

All crystallization trials were carried out by the vapour diffusion method at 20°C. PaMan5A was concentrated to 8 mg.ml⁻¹ in 20 mM Hepes pH 7.5, 150 mM NaCl buffer. Initial crystallization trials were performed using Wizard and MDL screens (Qiagen) on a cartesian robot. For each condition, three drops (100 nl of screen buffer + 100 nl, 200 nl and 300 nl of protein) were formed. Optimization was then carried out by varying the pH and the concentration of precipitant. The final crystallization conditions were: Tris 0.1 M pH 8.5, 0.2 M sodium acetate, 30% PEG 4000. Glycerol was used at a concentration of 25-30% as the cryoprotectant in the subsequent data collection stage. PaMan5A crystals belonged to the P2₁2₁2₁ space group with the following cell dimensions: a = 56.9Å, b = 58.0Å, c = 98.2Å and diffracted to 1.4Å resolution. X-ray diffraction data of a PaMan5A crystal were collected at 100K at the European Synchrotron Research Facilities (ESRF, Grenoble, France) beam line ID29.

PaMan26A was concentrated to ~ 26 mg.ml⁻¹ in 20 mM Hepes pH 7.5, 150 mM NaCl buffer. Small PaMan26A crystals were obtained in the conditions (i) 0.1 M Tris pH 7, 0.2 M Li₂SO₄, 1 M Potassium Sodium Tartrate and (ii) 0.1 M Imidazole pH 8, 0.1 M Potassium Sodium Tartrate, 0.2 M NaCl, both conditions of the Wizard screen. The best crystals were obtained after optimization in a solution containing 0.1 M Tris pH 7, 0.2 M NaCl, 0.8 M potassium sodium tartrate, 1 mM HgCl₂. For cryoprotection, crystals were transferred in a solution containing 25% (v/v) glycerol, 1.5 M Li₂SO₄, 100 mM bis-Tris propane pH 7.4. The crystals belonged to the P6₅22 space group with the following cell dimensions: a=b= 97.5Å, c = 268.7Å. Several X-ray diffraction data sets were collected on beam line Proxima1 at the French synchrotron SOLEIL (Saint-Aubin, France) and on beam lines ID14-4 and ID29 at the European Synchrotron Research Facilities (ESRF, Grenoble, France). The best X-ray diffraction data were collected to 2.85Å resolution at the European Synchrotron Research Facilities (ESRF, Grenoble, France) beam line ID14-4.

All the data sets were processed with the programs XDS (33) and SCALA (34). The data collection statistics are summarized in Table 2.

Structure determination and refinement

The structure of *PaMan5A* was determined with the molecular replacement method using the AMoRe program (35) and the *T. reesei* GH5 mannanase coordinates (PDB entry 1QNO). The rotation function yielded one solution, and the translation function yielded a unique solution, with a correlation coefficient and an R_{factor} of 38.1 and 44.5%, respectively, for data between 10 and 4 Å. After rigid body refinement, the correlation coefficient was 59.2% for an R_{factor} of 35.9%. After refinement using the programs Refmac (36) and Buster (37) the final crystallographic R_{factor} and R_{free} were 15.0 and 17.2%.

The structure of *PaMan26A* was also determined with the molecular replacement method using the AMoRe program (35). The superposition of 4 structures of GH26 CDs (PDB code: 2QHA, 2BVT, 2VX4 and 2WHK) plus the homology model given by the Phyre server (38) has been used as an ensemble search model for molecular replacement. The rotation function yielded one solution, and the translation function yielded a unique solution, with a correlation coefficient and an R_{factor} of 32.4 and 49.2%, respectively, for data between 10 and 4 Å. After rigid body refinement, the correlation coefficient was 42.7% for an R_{factor} of 43.7%. A modified structure of the CBM35 from *Clostridium thermocellum* (PDB 2W47) with most of the loops deleted was located manually in the difference Fourier electron density map and was used as a starting point to build the CBM domain of *PaMan26A*. After performing several cycles of refinement using Refmac (36) and Buster (37) programs and manual replacement and building on the graphic display with the Turbo-Frodo program (39), the R_{factor} has decreased to 20.7% (R_{free} 25.8%). All representations of the structure in the figures were prepared with the program PyMOL (<http://www.pymol.org/>). Coordinates for the structure *PaMan5A* and *PaMan26A* have been deposited in the Protein Data Bank under the accession number 3ZIZ and 3ZM8, respectively.

RESULTS AND DISCUSSION

Hydrolytic activity of *PaMan5A* and *PaMan26A* towards polysaccharides

In a recent study, we showed that *PaMan5A* and *PaMan26A* displayed similar kinetic parameters toward a range of mannan substrates. To further compare the *P. anserina* mannanases, we measured the release of manno-oligosaccharides following hydrolysis of ivory nut mannan and carob galactomannan. Towards the end of the reaction, *PaMan5A* yielded mainly M_2 and M_3 and smaller amount of M_1 (data not shown), consistent with other GH5 mannanases such as *T. reesei* (40). *PaMan26A* produced mainly M_4 , and smaller amounts of M_1 , M_2 and M_3 (data not shown). In other GH26 mannanases, different profiles have been observed: *C. fimi* CjMan26A and *C. japonicus* CjMan26B released M_2 and M_1 (17, 26) and *B. subtilis* z-2 BCMAN released M_2 and M_4 (21). The nature of oligosaccharide products released upon mannan hydrolysis confirms (i) the endo-mode of action of the two enzymes and (ii) differences between the two enzymes in substrate binding.

Hydrolytic activity of *PaMan5A* and *PaMan26A* towards oligosaccharides

The capacity of *PaMan5A* and *PaMan26A* to hydrolyze a range of manno-oligosaccharides was evaluated by ionic chromatography to get further insights into their active site architecture (Figure 1). *PaMan5A* had very low activity on M_3 , higher activity on M_4 and cleaved M_5 and M_6 rapidly (Table 3). A decrease of k_{cat}/K_M was observed with decreasing degree of polymerization (DP). The relative k_{cat}/K_M of *PaMan5A* on M_3 , M_4 , M_5 , and M_6 were 1: 358: 1127: 1782. The increase of the DP from 4 to 5 (M_4 and M_5) resulted in a 3.1-fold increase in k_{cat}/K_M , suggesting that at least four subsites are required to achieve efficient hydrolysis. In contrast, *PaMan26A* had no detectable activity on M_3 , very low activity on M_4 and cleaved M_5 and M_6 rapidly. For *PaMan26A* the relative k_{cat}/K_M on M_4 , M_5 , and M_6 were 1: 195: 365 with an increase of k_{cat}/K_M of 1.9-fold between M_5 and M_6 hydrolysis. These data suggest that *PaMan26A* requires at least five subsites to achieve maximum manno-oligosaccharide hydrolysis efficiency.

The nature of the hydrolysis products yielded from manno-oligosaccharides (summarized in Table 4) also revealed striking differences between the *P. anserina* mannanases. M_6 hydrolysis by *PaMan5A* produced mainly M_3 with smaller amounts of M_2 and M_4 , whereas M_6 hydrolysis by *PaMan26A* produced mainly

M₄ and M₂, with smaller amounts of M₅ and M₁, and without any M₃. M₅ hydrolysis by *PaMan5A* yielded mainly M₂ and M₃, with small amounts of M₄ and M₁, whereas hydrolysis by *PaMan26A* yielded only M₄ and M₁. M₄ hydrolysis by *PaMan5A* yielded mainly M₂ with small amounts of M₁ and M₃, whereas *PaMan26A* had low activity on M₄ and produced M₁, M₂ and M₃. *PaMan5A* hydrolysed poorly M₃ yielding M₁ and M₂ and *PaMan26A* had no detectable activity on M₃. Both mannanases had no detectable activity on M₂ and pNP-mannose even at high enzyme loading (data not shown). Again, *PaMan26A* showed an atypical hydrolytic profile for a GH26 endo-mannanase compared to *CfMan26A* and *CjMan26A*. *CjMan26A* hydrolyses M₄ rapidly and requires occupation of four subsites to achieve efficient hydrolysis (18), while *CfMan26A* is less efficient towards M₄ and requires substrate binding at five subsites to achieve efficient hydrolysis (17). For *PaMan26A*, the occupation by substrate of at least five subsites to achieve efficient hydrolytic activity is even more pronounced, with a dramatic increase in k_{cat}/K_M between M₄ and M₅.

Productive binding mode of M₅ and M₆ by PaMan5A and PaMan26A

β -Mannanases usually bind oligomeric substrates in multiple productive binding modes that can generate identical products. The simplest example of this is M₃ hydrolysis in to M₂ and M₁, where mannose would be released from either the reducing end or the non-reducing end. In the former case M₃ binds productively from the -1 subsite to the +2 subsite and in the latter case from the -2 to the +1 subsite, following the established subsite nomenclature (41). As another example, from M₅, each of the products M₃ and M₄ respectively, can be produced by either of two binding modes (see scheme in Figure 2A). Binding of M₅ from subsite -2 to +3 or from subsite -3 to +2 both generates M₃ and binding from subsite -4 to +1 and from subsite -1 to +4 both generates M₄. Thus, product analysis using HPAEC-PAD data alone can not distinguish between binding modes giving the same products. However, this can be achieved when the HPAEC-PAD product analysis (as in previous paragraph) is combined with *in situ* product isotope labeling using ¹⁸O-labeled

water followed by mass spectrometric analysis, as shown previously (31, 32).

Relative quantities of the produced M₃, M₄ and M₅ from the HPAEC-PAD data of M₅ and M₆ hydrolysis (Table 4) were used to calculate the relative molar distribution of these products (Table 4, values in brackets) and thus the frequencies of productive binding modes that give rise to these products could be estimated (Figure 2A, far left and far right column). MALDI-TOF-MS analysis was conducted to determine the ratio of non-labeled (¹⁶O) and labeled (¹⁸O) species of each product (light versus heavy M₃, M₄ or M₅), that was then used to estimate the relative frequency of the productive binding modes of M₅ and M₆ that give rise to these same products. The combined results of the HPAEC-PAD and MALDI-TOF-MS data are summarized in Figure 2A, showing the relative frequencies (%) of productive binding modes of M₅ and M₆. The calculation procedure is explained in Table S1. To exemplify, determined from HPAEC-PAD data (Table 4), 80% of the productive binding during the hydrolysis of M₅ by *PaMan5A* generated M₃. MALDI-TOF analysis then determined the ratio between the two binding modes that give M₃. The analysis gave a ratio of M₃/M₃¹⁸ of 1: 2.9 (Figure 2B), which shows that the enzyme binds M₅ preferably from subsite -3 to +2 to produce M₃, giving a 59% frequency of this binding mode (Figure 2A). Small amounts of M₁ and M₄ were also produced, and the ratio of M₄/M₄¹⁸ was 1 : 0.7. Hydrolysis of M₆ by *PaMan5A* produced mainly M₃ (55% binding frequency), but also smaller amounts of M₂ and M₄. The ratio of M₄/M₄¹⁸ was 1: 3.2, which shows that *PaMan5A* binds M₆ preferably from subsite -4 to +2 to produce M₄ (34% binding frequency). Hydrolysis of M₅ by *PaMan26A* yielded M₁ and M₄ with a M₄/M₄¹⁸ ratio of 1: 5.0 (Figure 2B), which shows that the enzyme binds M₅ preferentially from subsite -4 to +1 (83% binding frequency, see Figure 2A). For hydrolysis of M₆, major product ratio analysis showed that the ratio of M₄/M₄¹⁸ was 1: 10.8, which shows that *PaMan26A* prefers to bind M₆ from subsite -4 to +2 (69% binding frequency). The ratio of the minor product M₅/M₅¹⁸ was 1: 4.2, showing that the M₁ and M₅ are mainly produced without binding at the +2 subsite. Thus, these data reveal clear differences in the binding mode of the two *P. anserina* mannanases: the predominant mode of binding

of M₅ and M₆ were significantly different (Figure 2A). *PaMan5A* showed a classical pattern of hydrolysis products (M₃ and M₂ mainly were released from M₅) as described in several studies (*B. subtilis*, *C. japonicus*, *M. edulis*) whereas *PaMan26A* showed release of M₄ and M₁ from M₅, which is unusual when compared to other GH26 endo-mannanases (*B. subtilis* BcMan, *C. fimi* CfMan26A, *C. japonicus* CjMan26A), suggesting an unusual arrangement of subsites in the catalytic center.

Transglycosylation ability

In order to detect potential transglycosylation ability of the two enzymes, they were incubated with M₅ as substrate. The resulting short time course study of the product formation clearly showed that *PaMan5A* in addition to hydrolysis products also produces transglycosylation products with higher DP than the original substrate (Figure 3). *PaMan5A* was able to transglycosylate yielding to oligosaccharide structures of up to a DP of 8 (n+1 to n+3), in good agreement with GH5 mannanases described before, *T. reesei* (n+1 to n+3) (31), and *A. nidulans* ManA (n+1 to n+3) and ManC (n+1 and n+2) (6). No transglycosylation products could be detected with *PaMan26A* incubated with M₅ in the same experimental conditions, which is consistent with some other family GH26 mannanases that have been described as non transglycosylating enzymes (10).

Structure of *PaMan5A*

The crystal structure of *PaMan5A* was solved in its free form. The crystal contained 1 monomer in the asymmetric unit and light-scattering experiments indicated that the protein is a monomer in solution (data not shown). The overall structure of *PaMan5A* (Figure 4A) revealed a (β/α)₈-barrel fold as expected for enzymes belonging to clan GH-A. When superimposed with *TrMan5A* (PDB entry 1QNR) and *T. fusca* mannanase (PDB entry 3MAN) structures (Figure S1), the overall fold of *PaMan5A* is very similar to that of *TrMan5A*, with structural differences being confined mainly in the loop regions (Figure 4A) that have been defined as eight loops, loop 1 (residues 35 to 42), loop 2 (66 to 95), loop 3 (120 to 144), loop 4 (177 to 184), loop 5 (213 to 232), loop 6 (252 to 258), loop 7 (287 to 289) and loop 8 (316 to 336). Compared to *TrMan5A* that contains four disulfide bonds:

C26-C29, C172-C175, C265-C272 and C284-C334, *PaMan5A* contained only 3 disulfide bonds, i.e., C180-C184, C272-C279, C291-C342. Following N-deglycosylation of *PaMan5A* using PNGaseF, no shift in the apparent molecular mass (46 kDa) was observed on SDS-PAGE compared to untreated sample (data not shown). This observation was in good agreement with NetGlyc predictions from the *PaMan5A* primary sequence (no predicted N-glycosylation site) and analysis of the *PaMan5A* crystallographic data that confirmed absence of glycosylation units.

The active site of *PaMan5A* was clearly identified in the groove, with the two conserved catalytic glutamate residues (acid-base and nucleophile) positioned near the carboxy-terminal ends of β-strands four and seven of the (β/α)₈ barrel (41), E177 and E283, respectively. Mutant E283A showed no catalytic activity for glucomannan, thus indicating that E283 should be the nucleophile. E177A had a specific activity of 0.47 U.mg⁻¹ towards glucomannan, which is roughly 100-fold lower than the wild-type enzyme (45 U.mg⁻¹), thus indicating that E177 should be the acid-base catalytic residue. These results are in agreement with other homologous GH5 enzymes where catalytic residues have been determined (42, 43). Despite several attempts, no structure of *PaMan5A* inactive mutants alone or in complex with its substrate has been obtained. Consequently, we performed comparative structural analysis of *PaMan5A* with other GH5 mannanases complexes (*T. reesei* PDB 1QNO, *T. petrophila* PDB 3PZ9, and *S. lycopersicum* PDB 1RH9) to map the substrate binding subsites (Figure 4B). In the -1 and +1 subsites where the catalytic cleavage occurs, 7 out of 8 residues highly conserved in GH5 mannanases (44) are found in *PaMan5A*, among which the catalytic residues E177 and E283 and R62, N176, H248, Y250, W315 (Figure 4B). *PaMan5A* also has an arginine equivalent to R171 in the +2 subsite of *TrMan5A* (15), which is semi-conserved among GH5 mannanases, and that was shown to play a significant role in the transglycosylation ability of *TrMan5A* (32).

Structure of *PaMan26A* catalytic module

The structure of *PaMan26A* was successfully solved using molecular replacement. The search model was composed of the superimposition of four structures of bacterial

mannanases (PDB code: 2QHA, 2BVT, 2VX4 and 2WHK). The final structure comprising 443 residues was refined at 2.85Å resolution. The overall structure of *PaMan26A* CD revealed a (β/α)₈-barrel fold (Figure 5A) as expected for enzymes belonging to clan-GHA. The active site was clearly identified in the groove, with the two conserved catalytic glutamate residues (E300 and E390) positioned at the end of the (β/α)₈ barrel, and several aromatic residues forming the subsites of catalytic cleft. Mutant E390A showed no catalytic activity for glucomannan, indicating that E390 should be the nucleophile. E300A had a specific activity of 0.33 U.mg⁻¹, which is roughly 200-fold lower than the wild-type enzyme (65 U.mg⁻¹), thus indicating that E300 should be the acid-base catalytic residue. These results are in agreement with other homologous GH26 enzymes where catalytic residues have been determined (45).

Electron density was observed for two carbohydrate sugar residues at one glycosylation site, N268, which is located in the CD on the external side of the barrel. As modeled from the electron density, 2 β -1,4 linked N-acetylglucosamine (GlcNAc) units are attached to this N-glycosylation site. N-deglycosylation of *PaMan26A* using PNGaseF was associated with a 2-3 kDa shift in the apparent molecular mass on SDS-PAGE compared to untreated sample (data not shown). These results confirm that *PaMan26A* is N-glycosylated and are in agreement with the NetNGlyc prediction (one predicted N-glycosylation site at position N268).

Several regions are highly conserved between *PaMan26A* and other GH26 mannanases from *B. subtilis* z-2 (PDB 2QHA), *B. subtilis* subsp. *bacillus* (PDB 2WHK), *C. japonicus* (PDB 1GW1 and 2VX6), and *C. fimi* (PDB 2BVT; Figure S2) as shown superimposition of *PaMan26A* and *B. subtilis* z-2 (PDB 2QHA) structures (Figure 5A). The central β -barrel and most of the surrounding α -helices are superimposable between *PaMan26A* and *B. subtilis* z-2 while loop regions are dramatically different. Indeed, *B. subtilis* enzyme exhibits a flat surface with a shallow dish shaped active center whereas *PaMan26A* displays large loops that form a deep cleft. According to the three dimensional structure of *PaMan26A*, 8 loops are involved in the binding of the substrate to the active site: loop 1 (171 to 174), loop 2 (195 to 208), loop 3 (230 to 266), loop 4 (301 to

314), loop 5 (342 to 346), loop 6 (362 to 368), loop 7 (392 to 396) and loop 8 (413 to 425). The most striking difference stands in loop 2 that contains four aromatic residues (W244, W245, F248 and Y249) and is nine amino-acids longer than *B. subtilis* z-2 (PDB 2QHA), *B. subtilis* subsp. *bacillus* (PDB 2WHK), *C. japonicus* (PDB 2VX6) and *C. fimi* (PDB 2BVT) mannanases. A shorter loop 2 does not allow interaction with the substrate at the glycone binding subsites in the case of *B. subtilis* z-2 (PDB 2QHA). The -1 and +1 subsites of *PaMan26A* are quite similar to homologous enzymes with the conserved residues H299, W305, F306, Y362, W413 (Figures 5B and 5C). As described for *CfMan26A* and *CjMan26A*, *PaMan26A* Y362 is probably involved in a hydrogen bond with the catalytic nucleophile E390, while *PaMan26A* W305 and W413 could play a role as aromatic platforms to stabilize mannopyranose rings at the +1 and -1 subsites, respectively (Figure 5C). In the -2 subsite of BcMan, binding is not favorable because of steric hindrance due to the position of Y40 (21). In the case of *CfMan26A*, the two aromatic F123 and Y124 residues that are superimposed with *PaMan26A* F248 and Y249, stabilize the interaction with a mannose unit at the -2 subsite (Figure 5C).

Our experimental data indicate that *PaMan26A* displays strong interactions at the -4 subsite. Indeed, *PaMan26A* was poorly active toward M₄ probably due to the formation of an unproductive complex between -4 and -1 subsites. We further analyzed the -4 subsite in the *PaMan26A* structure and identified two aromatic residues, W244 and W245, located in loop 2 that could stabilize mannopyranose rings in the -4 subsite (Figures 5B and 5C). As *PaMan26A*, *CfMan26A* active site also contains four glycone binding subsites but experimental results provided evidence for the existence of a strong -3 subsite and residues involved in -4 were described as making a minor contribution to binding (17). In *PaMan26A*, there is no equivalent to the F42, F325 and Q329 *CfMan26A* -3 subsite residues. The lack of a strong -3 subsite and the presence of a strong -4 subsite in the structure is in agreement with our experimental results that suggest a predominant substrate binding mode involving the -4 subsite. Lacking a strong -4 subsite, *CfMan26A* produces M₂ and M₃ as

major products from M₅ with only minor amount of M₁ and M₄ (31).

PaMan26A modular organization

PaMan26A harbors a family 35 CBM at its N-terminal end, and the closest characterized enzyme is *Humicola insolens* β -mannanase (GenBank AAQ31840, (46)) with 78% amino-acid identity. Following a BlastP search using PaMan26A amino-acid sequence, it is interesting to note that all related bacterial and fungal sequences harbor a CBM35 module at their N-terminus. In fungi, in addition to PaMan26A CBM35, only one CBM35 module binding to galactan has been characterized to date in a *Phanerochaete chrysosporium* exo- β -1,3-galactanase (47). We previously suggested that the N-terminal CBM35 module of PaMan26A displayed dual binding specificity toward xylan and mannan (28) and the phylogenetic analysis performed by (48) clustered PaCBM35 in the subfamily II that is proposed to target β -1,4 mannan.

While the structures of fungal GH bearing a CBM are generally determined separately, this is the first intact structure that allows visualization of the juxtaposition of the CBM35 module relative to the GH26 CD. The linker region of PaMan26A is short without any glycosylation sites while modular fungal GHs usually display long and highly glycosylated linkers. The PaMan26A linker sequence was rich in proline residues, i.e., it contains 4 prolines (P132, P134, P135 and P140) out of 12 residues that may confer rigidity to the modular enzyme (Figure 6A). The linker starts on residue S130 at the end of the last β -strand of the N-terminal CBM domain. Only 2 residues (A131 and P132) have no interaction with the rest of the molecule. The region from residue R133 to residue N141, which may be considered as the end of the linker, is tightly bound to the CD. R133 and H136 side chains make hydrogen bond with D382, N374 and Q404 while the side chain of I138 fits into a hydrophobic cavity made of R159 (aliphatic part of the side chain), Y162 and M385. The CBM and the catalytic module are thus in close association thanks to the embedded linker (Figure 6B) and it may explain why attempts to express the catalytic module alone were unsuccessful (data not shown). Alignment of PaMan26A-CBM35 with 60 microbial GH26 mannanases sequences bearing a CBM35 module revealed that they all display a short

linker region (12-14 residues) rich in proline residues (data not shown).

The CBM35 domain comes into contact with the CD through hydrophobic interactions. Indeed a hydrophobic patch comprising L58 and L103 on the surface of the CBM35 domain stands in front of a cluster of hydrophobic residues (A402, Y403 and L399) of the CD.

The rationale of the tight modular association of bacterial and fungal GH26-CBM35 mannanases will need further work to gain insights into their function.

PaCBM35 domain

The CBM35 domain overall structure consists of 2 antiparallel sheets consisting of 4 and 5 antiparallel β -strands, respectively. The two sheets are packed in a β -sandwich conformation enclosing a highly hydrophobic core. The closest structural homologue found using the DALI server (49) is a CBM35 from *Clostridium thermocellum* (PDB code 2W1W, (50)), with a Z-score of 18.6. Its superimposition with PaCBM35 shows that 57 C α out of 125 C α (45%) have equivalent positions in both molecules, with the distance between the superimposed C α atoms being < 1Å. The main differences occur in the loops connecting the beta-strands as shown in Figure 6C. A metal ion is present, which has been modeled as calcium, based on its coordination geometry exclusively with oxygen atoms. A calcium ion is also present at a similar location in the structure of the CBM35 domain from *C. thermocellum* (50). However, the second calcium evidenced in all of the other CBM35s and involved in carbohydrate recognition (50) is not conserved in PaCBM35. A platform of three aromatic residues (F87, W117 and W119) was observed at the surface of the PaCBM35 (Figure 6B). These residues are aligned with the PaMan26A catalytic cleft suggesting that they could play a role in substrate binding.

Conclusions

The *P. anserina* CAZome (the genome-wide inventory of CAZymes) includes three genes encoding β -(1,4)-mannanases (www.cazy.org): two GH5 mannanases without CBM (including PaMan5A) that both belong to the GH5 subfamily 7 (51) and one GH26 mannanase bearing a CBM35 (i.e., PaMan26A) with affinity for hemicellulosic polysaccharides (28). Based on our kinetic analysis, we can

conclude that *PaMan5A* and *PaMan26A* are complementary in terms of hydrolysis profile and could act in synergy to deconstruct mannan polysaccharides. Indeed, *PaMan26A* produces larger manno-oligosaccharides that could be processed by *PaMan5A*. In *C. japonicus*, a bacterium also producing both GH5 and GH26 β -mannanases, the catalytic modules of GH5 mannanases were linked to various CBMs whereas GH26 mannanases were found as single CD (25). Therefore it has been suggested that GH26 mannanases were involved in degradation of storage tissues whereas GH5 mannanases harboring cellulose-specific CBMs were involved in degradation of plant cell-wall (20, 26). It is interesting to note that the *P. anserina* mannanase system does not seem to fit with this model, suggesting a difference in

the strategies to degrade mannan between these two microbes.

Together with our previous studies on *P. anserina* CAZymes (28, 52, 53), the present findings give more insights into *P. anserina*'s enzymatic machinery for the deconstruction of plant cell wall polysaccharides. This knowledge is essential to design tailor-made biocatalysts, which can then be used in the biofuel and bioprocessing industries.

REFERENCES

1. Timell, T. E. (1967) Recent progress in the chemistry of wood hemicellulose. *Wood Sci Technol* **1**, 45-70
2. Cantarel, B.L., Coutinho, P. M., Rancurel, C., Bernard, T., Lombard, V., and Henrissat, B. (2009) The Carbohydrate-Active EnZymes database (CAZy): an expert resource for glycogenomics. *Nucleic Acids Res* **37**, 233-238
3. Davies, G., and Henrissat, B. (1995) Structures and mechanisms of glycosyl hydrolases. *Structure* **3**, 853-859
4. Vocadlo, D. J., and Davies, G. J. (2008) Mechanistic insights into glycosidase chemistry. *Curr Opin Chem Biol* **12**, 539-555
5. Gilbert, H. J., Stålbrand, H., and Brumer, H. (2008) How the walls come crumbling down: recent structural biochemistry of plant polysaccharide degradation. *Curr Opin Plant Biol* **11**, 338-348
6. Dilokpimol, A., Nakai, H., Gotfredsen, C. H., Baumann, M. J., Nakai, N., Abou Hachem, M., and Svensson, B. (2011) Recombinant production and characterisation of two related GH5 endo- β -1,4-mannanases from *Aspergillus nidulans* FGSC A4 showing distinctly different transglycosylation capacity. *Biochem Biophys Acta* **1814**, 1720-1729
7. Larsson, A. M., Anderson, L., Xu, B., Muñoz, I. G., Usón, I., Janson, J. C., Stålbrand, H., and Ståhlberg, J. (2006) Three-dimensional crystal structure and enzymic characterization of beta-mannanase Man5A from blue mussel *Mytilus edulis*. *J Mol Biol* **357**, 1500-1510
8. Harjunpää, V., Helin, J., Koivula, A., Siika-aho, M., and Drakenberg, T. (1999) A comparative study of two retaining enzymes of *Trichoderma reesei*: transglycosylation of oligosaccharides catalysed by the cellobiohydrolase I, Cel7A, and the beta-mannanase, Man5A. *FEBS Lett* **443**, 149-153
9. Zhang, Y., Ju, J., Peng, H., Gao, F., Zhou, C., Zeng, Y., Xue, Y., Li, Y., Henrissat, B., Gao, G. F., and Ma, Y. (2008) Biochemical and structural characterization of the intracellular mannanase AaManA of *Alicyclobacillus acidocaldarius* reveals a novel glycoside hydrolase family belonging to clan GH-A. *J Biol Chem* **283**, 31551-31558
10. Anderson, L., Häggglund, P., Stoll, D., Lo Leggio, L., Drakenberg, T. and Stålbrand, H. (2008) Kinetics and stereochemistry of the *Cellulomonas fimi* β -mannanase studied using ¹H-NMR. *Biocatal Biotransfor* **26**, 86-95
11. Stoll, D., Boraston, A., Stålbrand, H., McLean, B. W., Kilburn, D. G., Warren, R. A. (2000) Mannanase Man26A from *Cellulomonas fimi* has a mannan-binding module. *FEMS Microbiol Lett* **183**, 265-269
12. Häggglund, P., Eriksson, T., Collén, A., Nerinckx, W., Claeysens, M., and Stålbrand, H. (2003) A cellulose-binding module of the *Trichoderma reesei* beta-mannanase Man5A increases the mannan-hydrolysis of complex substrates. *J Biotechnol* **101**, 37-48
13. Fujimoto, Z., Kuno, A., Kaneko, S., Kobayashi, H., Kusakabe, I., and Mizuno, H. (2002) Crystal structures of the sugar complexes of *Streptomyces olivaceoviridis* E-86 xylanase: sugar binding structure of the family 13 carbohydrate binding module. *J Mol Biol* **316**, 65-78
14. Pell, G., Szabo, L., Charnock, S. J., Xie, H., Gloster, T. M., Davies, G. J., and Gilbert, H. J. (2004) Structural and biochemical analysis of *Cellvibrio japonicus* xylanase 10C: how variation in substrate-binding cleft influences the catalytic profile of family GH-10 xylanases. *J Biol Chem* **279**, 11777-11788
15. Sabini, E., Schubert, H., Murshudov, G., Wilson, K. S., Siika-Aho, M., Penttilä, M. (2000) The three-dimensional structure of a *Trichoderma reesei* beta-mannanase from glycoside hydrolase family 5. *Acta Crystallogr D Biol Crystallogr* **56**, 3-13
16. Bourgault, R., Oakley, A. J., Bewley, J. D., and Wilce, M. C. (2005) Three-dimensional structure of (1,4)-beta-D-mannan mannanohydrolase from tomato fruit. *Protein Sci* **14**, 1233-1241
17. Le Nours, J., Anderson, L., Stoll, D., Stålbrand, H., and Lo Leggio, L. (2005) The structure and characterization of a modular endo-beta-1,4-mannanase from *Cellulomonas fimi*. *Biochemistry* **44**, 12700-12708
18. Hogg, D., Woo, E. J., Bolam, D. N., McKie, V. A., Gilbert, H. J., and Pickersgill, R. W. (2001) Crystal structure of mannanase 26A from *Pseudomonas cellulosa* and analysis of residues involved in substrate binding. *J Biol Chem* **276**, 31186-31192

19. Fanutti, C., Ponyi, T., Black, G. W., Hazlewood, G.P., and Gilbert, H. J. (1995) The conserved noncatalytic 40-residue sequence in cellulases and hemicellulases from anaerobic fungi functions as a protein docking domain. *J Biol Chem* **270**, 29314-29322
20. Tailford, L. E., Ducros, V. M., Flint, J. E., Roberts, S. M., Morland, C., Zechel, D. L., Smith, N., Bjørnvad, M. E., Borchert, T. V., Wilson, K. S., Davies, G. J., and Gilbert, H. J. (2009) Understanding how diverse beta-mannanases recognize heterogeneous substrates. *Biochemistry* **48**, 7009-1018
21. Yan, X. X., An, X. M., Gui, L. L., and Liang, D. C. (2008) From structure to function: insights into the catalytic substrate specificity and thermostability displayed by *Bacillus subtilis* mannanase BCman. *J Mol Biol* **379**, 535-544
22. Ducros, V. M., Zechel, D. L., Murshudov, G.N., Gilbert, H.J., Szabó, L., Stoll, D., Withers, S.G., and Davies, G.J. (2002) Substrate distortion by a beta-mannanase: snapshots of the Michaelis and covalent-intermediate complexes suggest a B(2,5) conformation for the transition state. *Angew Chem Int Ed Engl* **41**, 2824-2827
23. Cartmell, A., Topakas, E., Ducros, V. M., Suits, M. D., Davies, G. J., and Gilbert, H. J. (2008) The *Cellvibrio japonicus* mannanase CjMan26C displays a unique exo-mode of action that is conferred by subtle changes to the distal region of the active site. *J Biol Chem* **283**, 34403-34413
24. Setati, M. E., Ademark, P., van Zyl, W., Hahn-Hägerdal, B., and Stålbrand, H. (2001) Expression of the *Aspergillus aculeatus* Endo- β -1,4-mannanase Encoding Gene (man1) in *Saccharomyces cerevisiae* and Characterization of the recombinant Enzyme. *Protein Expr Purif* **21**, 105-114
25. Xu, B., Hägglund, P., Stålbrand, H., and Janson, J. C. (2002) endo- β -1,4-Mannanases from blue mussel *Mytilus edulis*: purification, characterization, and mode of action. *J Biotechnol* **92**, 267-277
26. Hogg, D., Pell, G., Dupree, P., Goubet, F., Martin-Orúe, S. M., Armand, S., Gilbert, H. J. (2003) The modular architecture of *Cellvibrio japonicus* mannanases in glycoside hydrolase families 5 and 26 points to differences in their role in mannan degradation. *Biochem J* **371**, 1027-1043
27. Espagne, E., Lespinet, O., Malagnac, F., Da Silva, C., Jaillon, O., Porcel, B. M., Couloux, A., Aury, J. M., Ségurens, B., Poulain, J., Anthouard, V., Grossetete, S., Khalili, H., Coppin, E., Déquard-Chablat, M., Picard, M., Contamine, V., Arnaise, S., Bourdais, A., Berteaux-Lecellier, V., Gautheret, D., de Vries, R. P., Battaglia, E., Coutinho, P. M., Danchin, E. G., Henrissat, B., Khoury, R. E., Sainsard-Chanet, A., Boivin, A., Pinan-Lucarré, B., Sellem, C. H., Debuchy, R., Wincker, P., Weissenbach, J., and Silar, P. (2008) The genome sequence of the model ascomycete fungus *Podospora anserina*. *Genome Biol* **9**, R77
28. Couturier, M., Haon, M., Coutinho, P. M., Henrissat, B., Lesage-Meessen, L., Berrin, J-G. (2011) *Podospora anserina* hemicellulases potentiate the *Trichoderma reesei* secretome for saccharification of lignocellulosic biomass. *Appl Environ Microbiol* **77**, 237-246
29. Matsui, I., Ishikawa, K., Matsui, E., Miyairi, S., Fukui, S., and Honda, K. (1991) Subsite structure of *Saccharomycopsis* alpha-amylase secreted from *Saccharomyces cerevisiae*. *J Biochem* **109**, 566-569
30. Berrin, J-G., el Ajandouz, H., Georis, J., Arnaut, F., and Juge, N. (2007) Substrate and product hydrolysis specificity in family 11 glycoside hydrolase: an analysis of *Penicillium funiculosum* and *Penicillium griseofulvum* xylanases. *Appl Microbiol Biotechnol* **74**, 1001-1010
31. Hekmat, O., Lo Leggio, L., Rosengren, A., Kamarauskaite, J., Kolenova, K., and Stålbrand, H. (2010) Rational engineering of mannosyl binding in the distal glycone subsites of *Cellulomonas fimi* endo-beta-1,4-mannanase: mannosyl binding promoted at subsite -2 and demoted at subsite -3. *Biochemistry* **49**, 4884-4896
32. Rosengren, A., Hägglund, P., Anderson, L., Pavon-Orozco, P., Peterson-Wulff, R., Nerinckx, W., and Stålbrand, H. (2012) The role of subsite +2 of the *Trichoderma reesei* β -mannanase TrMan5A in hydrolysis and transglycosylation. *Biocatal Biotransfor* **30**, 338-352
33. Kabsch, W. (2010) XDS. *Acta Crystallogr D Biol Crystallogr* **66**, 125-132
34. Evans, P. (2006) Scaling and assessment of data quality. *Acta Crystallogr D Biol Crystallogr* **62**, 72-82
35. Navaza, J. (2001) Implementation of molecular replacement in AMoRe. *Acta Crystallogr D Biol Crystallogr* **57**, 1367-1372

36. Murshudov, G. N., Vagin, A. A., and Dodson, E. J. (1997) Refinement of macromolecular structures by the maximum-likelihood method. *Acta Crystallogr D Biol Crystallogr* **53**, 240-255
37. Bricogne, G., Blanc, E., Brandl, M., Flensburg, C., Keller, P., Paciorek, W., Roversi, P., Sharff, A., Smart, O. S., Vornrhein, C., and Womack, T. O. (2011) BUSTER version 2.11.2
38. Kelley, L. A., and Sternberg, M. J. (2009) Protein structure prediction on the web: a case study using the Phyre server. *Nat Protocols* **4**, 363-371
39. Roussel, A., and Cambillau, C. (1991) Turbo-Frodo. in *Silicon Graphics Geometry Partners Directory*, Mountain View Pub., CA. pp 86
40. Stålbrand, H., Siika-aho, M., Tenkanen, M., Viikari, L. (1993) Purification and characterization of two β -mannanases from *Trichoderma reesei*. *J Biotechnol* **29**, 229-242
41. Davies, G. J., Wilson, K. S., and Henrissat, B. (1997) Nomenclature for sugar-binding subsites in glycosyl hydrolases. *Biochem J* **321**, 557-559
42. Jenkins, J., Lo Leggio, L., Harris, G., and Pickersgill, R. (1995) Beta-glucosidase, beta-galactosidase, family A cellulases, family F xylanases and two barley glycanases form a superfamily of enzymes with 8-fold beta/alpha architecture and with two conserved glutamates near the carboxy-terminal ends of beta-strands four and seven. *FEBS Lett* **362**, 281-285
43. Henrissat, B., Callebaut, I., Fabrega, S., Lehn, P., Mornon, J. P., and Davies, G. (1996) Conserved catalytic machinery and the prediction of a common fold for several families of glycosyl hydrolases. *Proc Natl Acad Sci U S A* **93**, 5674
44. Hilge, M., Gloor, S., Winterhalter, K., Zimmermann, W., and Piontek, K. (1996) Crystallization and preliminary crystallographic analysis of two beta-mannanase isoforms from *Thermomonospora fusca* KW3. *Acta Crystallogr D Biol Crystallogr* **52**, 1224-1225
45. Bolam, D. N., Hughes, N., Virden, R., Lakey, J. H., Hazlewood, G. P., Henrissat, B., Braithwaite, K. L., and Gilbert, H. J. (1996) Mannanase A from *Pseudomonas fluorescens ssp. cellulosa* is a retaining glycosyl hydrolase in which E212 and E320 are the putative catalytic residues. *Biochemistry* **35**, 16195-16204
46. Kauppinen, M. S., Schulein, M., Schnorr, K., Andersen, L. N., and Mads E. (1993) Mannanases Patent US 6566114
47. Ichinose, H., Yoshida, M., Kotake, T., Kuno, A., Igarashi, K., Tsumuraya, Y., Samejima, M., Hirabayashi, J., Kobayashi, H., and Kaneko, S. (2005) An exo-beta-1,3-galactanase having a novel beta-1,3-galactan-binding module from *Phanerochaete chrysosporium*. *J Biol Chem* **280**, 25820-25829
48. Correia, M. A., Abbott, D. W., Gloster, T. M., Fernandes, V. O., Prates, J. A., Montanier, C., Dumon, C., Williamson, M. P., Tunnicliffe, R. B., Liu, Z., Flint, J. E., Davies, G. J., Henrissat, B., Coutinho, P. M., Fontes, C. M., and Gilbert, H. J. (2010) Signature active site architectures illuminate the molecular basis for ligand specificity in family 35 carbohydrate binding module. *Biochemistry* **49**, 6193-6205
49. Holm, L., Rosenström, P. (2010) Dali server: conservation mapping in 3D. *Nucl Acids Res* **38**, W545-549
50. Montanier, C., van Bueren, A. L., Dumon, C., Flint, J. E., Correia, M. A., Prates, J. A., Firbank, S. J., Lewis, R. J., Grondin, G. G., Ghinet, M. G., Gloster, T. M., Herve, C., Knox, J. P., Talbot, B. G., Turkenburg, J. P., Kerovuo, J., Brzezinski, R., Fontes, C. M., Davies, G. J., Boraston, A. B., Gilbert, H. J. (2009) Evidence that family 35 carbohydrate binding modules display conserved specificity but divergent function. *Proc Natl Acad Sci U S A* **106**, 3065-3070
51. Aspeborg, H., Coutinho, P. M., Wang, Y., Brumer, H. 3rd, and Henrissat, B. (2012) Evolution, substrate specificity and subfamily classification of glycoside hydrolase family 5 (GH5). *BMC Evol Biol* **12**:186
52. Bey, M., Zhou, S., Poidevin, L., Henrissat, B., Coutinho, P. M., Berrin, J-G., Sigoillot, J-C. (2013) Cello-Oligosaccharide Oxidation Reveals Differences between Two Lytic Polysaccharide Monooxygenases (Family GH61) from *Podospira anserina*. *Appl Environ Microbiol* **79**, 488-496
53. Lafond, M., Navarro, D., Haon, M., Couturier, M., Berrin, J-G. (2012) Characterization of a broad-specificity β -glucanase acting on β -(1,3)-, β -(1,4)-, and β -(1,6)-glucans that defines a new glycoside hydrolase family. *Appl Environ Microbiol* **78**, 8540-8546

Acknowledgments—We thank N. Lopes-Ferreira, P.M. Coutinho and C. Dumon for helpful discussions, A. Blanchard for Dionex analyses and M. Haon for protein purification. We thank the European Synchrotron Radiation Facility (ESRF) at Grenoble (France) in particular the beamline ID29 staff and French synchrotron (SOLEIL) at Saint-Aubin (France) and the beamline Proxima1 staff for their assistance.

FOOTNOTES

*This study was funded by the FUTUROL project and OSEO Innovation. HS thanks FORMAS and VINNOVA for research funding.

¹To whom correspondence should be addressed: INRA, UMR1163 BCF, Aix Marseille Université, Polytech Marseille, F-13288 Marseille, France, Tel: +33(0)4 91 82 86 04; Fax: +33(0)4 91 82 86 01; E-mail: jean-guy.berrin@univ-amu.fr

²Architecture et Fonction des Macromolécules Biologiques, Aix Marseille Université, CNRS UMR7257, F-13288 Marseille, France

³Department of Biochemistry and Structural Biology, Lund University, P.O. Box 124, S-221 00, Lund, Sweden

⁴The abbreviations used are: CBM, Carbohydrate-Binding Module; CD, Catalytic Domain; DHB, 2,5-dihydroxybenzoic acid; DP, degree of polymerization; GH, Glycoside Hydrolase; HPAEC-PAD, High Performance Anion Exchange Chromatography-Pulsed Amperometric Detection; MALDI-TOF-MS, Matrix-Assisted Laser Desorption Ionization-Time-of-Flight Mass Spectrometry, M₁, mannose; M₂, mannobiose; M₃, mannotriose; M₄, mannotetraose; M₅, mannopentaose; M₆, mannohexaose *PaCBM35*, *Podospira anserina* CBM35; *PaMan5A*, *Podospira anserina* GH5 mannanase A; *PaMan26A*, *Podospira anserina* GH26 mannanase A

FIGURE LEGENDS

FIGURE 1: Progress curve of the manno-oligosaccharides generated by *PaMan5A* and *PaMan26A* after the hydrolysis of manno-oligosaccharides.

The recombinant enzymes were incubated with 100 μ M manno-oligosaccharides in acetate buffer pH 5.2 at 40°C. The quantity of mannose (open diamond), M₂ (open squared), M₃ (full circle), M₄ (full triangle), M₅ (full diamond), and M₆ (full squares) produced during the course of the reaction was quantified using HPAEC-PAD. The concentrations of enzymes used were *PaMan5A* (A) 18.2 nM with M₆, (B) 18.2 nM with M₅ and (C) 60 nM with M₄; *PaMan26A* (D) 15 nM with M₆ and (E) 30 nM with M₅.

FIGURE 2: Relative frequency of the productive modes of binding of manno-oligosaccharides to *PaMan5A* and *PaMan26A*. A. The numbers represent the percentages of binding in each binding mode. These were calculated from the quantitative product analysis using HPAEC-PAD (numbers to the far left and far right, obtained from Table 4) followed by a detailed analysis of the hydrolytic cleavage patterns of M₅ and M₆ using MALDI-TOF-MS analysis of ¹⁸O-labeled products, allowing to distinguish further between binding modes (numbers in bold). The arrow indicates the mannosidic bond to be cleaved. * = reducing end of oligosaccharide. The -4 and +3 dashed subsites are only present in *PaMan26A* and *PaMan5A*, respectively. ND = not detected. B. MALDI-TOF-MS spectra of M₅ hydrolysis by *PaMan5A* and *PaMan26A*, showing enlarged parts of the spectra with the M₃ product formed by *PaMan5A* at a ratio of 1: 2.9 of M₃/M₃¹⁸ (left) and the M₄ product formed by *PaMan26A* at a ratio of 1: 5.0 of M₄/M₄¹⁸ (right). The peaks in the spectra correspond to the monoisotopic masses of sodium adducts [M + Na]⁺ of the manno-oligosaccharides.

FIGURE 3: MALDI-TOF-MS analysis of the transglycosylation product formation from M₅ during 1-10 min by *PaMan5A*.

Peaks in the spectra correspond to monoisotopic masses of sodium adducts [M + Na]⁺ of manno-oligosaccharides: M₂: m/z 365.1, M₃: m/z 527.1, M₄: m/z 689.2, M₅: m/z 851.2, M₆: m/z 1013.3, M₇: m/z 1175.3 and M₈: m/z 1337.3. The enlarged part in each spectrum corresponds to approximately 3 % of the relative intensity.

FIGURE 4: Crystal structure of *PaMan5A*.

A: Superposition of *PaMan5A* (green) and *TrMan5A* (yellow) structures. The two views are related by a rotation of approximately 90° about the vertical axis. B: Surface view of the catalytic cleft of *PaMan5A* with mannotriose modeled in the -2 and -3 subsites and mannobiose modeled in the +1 and +2 subsites. The structures of GH5 from *T. reesei* and *T. fusca* in complex with mannobiose and mannotriose, respectively, were superimposed on the top of the structure of *PaMan5A* to map the substrate-binding subsites.

FIGURE 5: Crystal structure of *PaMan26A*.

A: Superposition of *PaMan26A* catalytic module (green) and *BcMan* (orange) structures. The two views are related by a rotation of approximately 90° about the vertical axis. B: Surface view of the catalytic cleft of *PaMan26A* with mannotriose modeled in the -2 to -4 subsites. The structure of GH26 from *C. fimi* in complex with mannotriose was superimposed on the top of the structure of *PaMan26A* to map the substrate-binding subsites. C: Organization of the glycone binding subsites in *PaMan26A* (yellow) compared with *C. fimi* (cyan).

FIGURE 6: Views of Modular architecture of *PaMan26A*.

A: Ribbon diagram of *PaMan26A* catalytic (blue) and CBM (green) domains. The proline-rich linker is shown in stick format. B: Molecular surface representation of *PaMan26A* structure with the catalytic domain in blue, the *PaCBM35* domain in green and the linker in purple. The three aromatic residues present at the surface of the *PaCBM35* domain are shown in yellow. C: Superposition of *PaCBM35* domain (green) and *C. thermocellum* CBM35 (orange). The calcium ion is represented by a blue sphere.

TABLES

Table 1: Mutagenesis primers used in the study

Primer	Nucleotide sequence 5' to 3' ^a
E177AFor	GGGAACCTTGCCAACGCGCCAGGTGCAAGGG
E177ARev	CCCTTGACCTGGGCGCGTTGGCAAGTTCCC
E283AFor	CCGTGTTTGTGGAGGCGTATGGGTATGAGAGTGATAGG
E283ARev	CCTATCACTCTCATACCCATACGCTCCAACAAACACGG
E320AFor	GGAGACCTCTTCACGCCGCGAGGGTGGTTGG
E320ARev	CCAACCACCTCCGCGGCGTGAAGAGGTCTCC
E410AFor	GATGATTGCTGCTGCAGCCGTTGGCGCTGCC
E410ARev	GGCAGCGCCAACGGCTGCAGCAGCAATCATC

^aModified codons are underlined

Table 2: Data collection and model refinement statistics of *PaMan5A* and *PaMan26A*

	<i>PaMan5A</i>	<i>PaMan26A</i>
<i>Data collection</i>		
Wavelength (Å)	0.97914	1.00648
Space group	P2 ₁ 2 ₁ 2 ₁	P6 ₅ 22
<i>a</i> , <i>b</i> , <i>c</i> (Å)	56.87, 57.90, 97.86	97.49, 97.49, 268.72
Resolution (Å) ^a	30-1.4 (1.48-1.4)	50-2.85 (3.0-2.85)
Unique reflections ^a	62,519 (8,848)	18,575 (2,627)
Multiplicity ^a	8.4 (8.3)	11.8 (11.8)
Completeness (%) ^a	97.3 (95.7)	99.9 (100.0)
I/σ ^a	18.7 (3.4)	25.6 (4.6)
R _{merge} (%) ^{a,b}	8.6 (67.8)	7.6 (65.2)
<i>Refinement and model quality</i>		
Resolution (Å)	30-1.4	30-2.85

Reflections	59,254	18,483
R _{cryst} /R _{free} (%) ^c	15.0/17.2	20.6/25.7
Number of atoms	3,193	3,676
Protein/carbohydrate moiety	2,745/0	3,493/28
Water/solvent/ion	434/14/0/	143/12/2
Average B-factors (Å ²)		
Protein/carbohydrate moiety	10.6	68.2/888
Water/solvent/ion	28.5/10.6	63.3/85.1/92.1
Rmsd ^d		
Bond (Å)	0.010	0.008
Angle (°)	1.02	1.04
Ramachandran plot (%)		
Most favoured regions	98.0	95.5
Additionally allowed regions	2.0	4.3
Outlier regions	0	0.2
PDB accession code	3ZIZ	3ZM8

^a Values in parentheses are for the highest-resolution shell.

^b $R_{\text{merge}} = \sum_{\text{hkl}} (\sum_i |I_{\text{hkl}} - \langle I_{\text{hkl}} \rangle|) / \sum_{\text{hkl}} \langle I_{\text{hkl}} \rangle$.

^c $R_{\text{cryst}} = \sum_{\text{hkl}} ||F_o| - |F_c|| / \sum_{\text{hkl}} |F_o|$; R_{free} is calculated for 5% of randomly selected reflections excluded from refinement.

^d Root mean square deviation from ideal values.

Table 3: Catalytic efficiencies of *PaMan5A* and *PaMan26A* on manno-oligosaccharides

Substrate	k_{cat}/K_M (M ⁻¹ min ⁻¹)	
	<i>PaMan5A</i>	<i>PaMan26A</i>
M ₆	2.9 x 10 ⁶	2.4 x 10 ⁶
M ₅	1.9 x 10 ⁶	1.3 x 10 ⁶
M ₄	5.9 x 10 ⁵	6.4 x 10 ³
M ₃	1.6 x 10 ³	ND

ND: Not determined due to low activity.

Table 4: Hydrolysis products released by *PaMan5A* and *PaMan26A* from manno-oligosaccharides

	Enzyme loading (nM)	Substrate	Products (μM)				
			M ₁	M ₂	M ₃	M ₄	M ₅
<i>PaMan5A</i>	60	M ₄	11	49	21	-	-
	18.2	M ₅	2	32	20 (80*)	5 (20*)	-
	18.2	M ₆	n.d.	12	34 (55*)	14 (45*)	n.d.
<i>PaMan26A</i>	30	M ₅	34	n.d.	n.d.	43 (100*)	-
	15	M ₆	13	28	n.d.	33 (75*)	11 (25*)

Products were quantified using HPAEC-PAD and are expressed in μM. Incubation was carried out for 30 minutes at 40°C; n.d., not detected. *The values in brackets represent the relative molar distribution (%) between the products M₃, M₄ and M₅ from each of the M₅ and M₆ incubations, which were used to estimate the relative frequency of productive binding modes yielding these products (presented in Figure 2A). One product (M₃, M₄ or M₅) per productive binding was used for calculations, thus only half of the produced M₃ (**bold**) from M₆ incubations was accounted for (two molecules of M₃ are produced from each molecule of M₆).

Figure 1

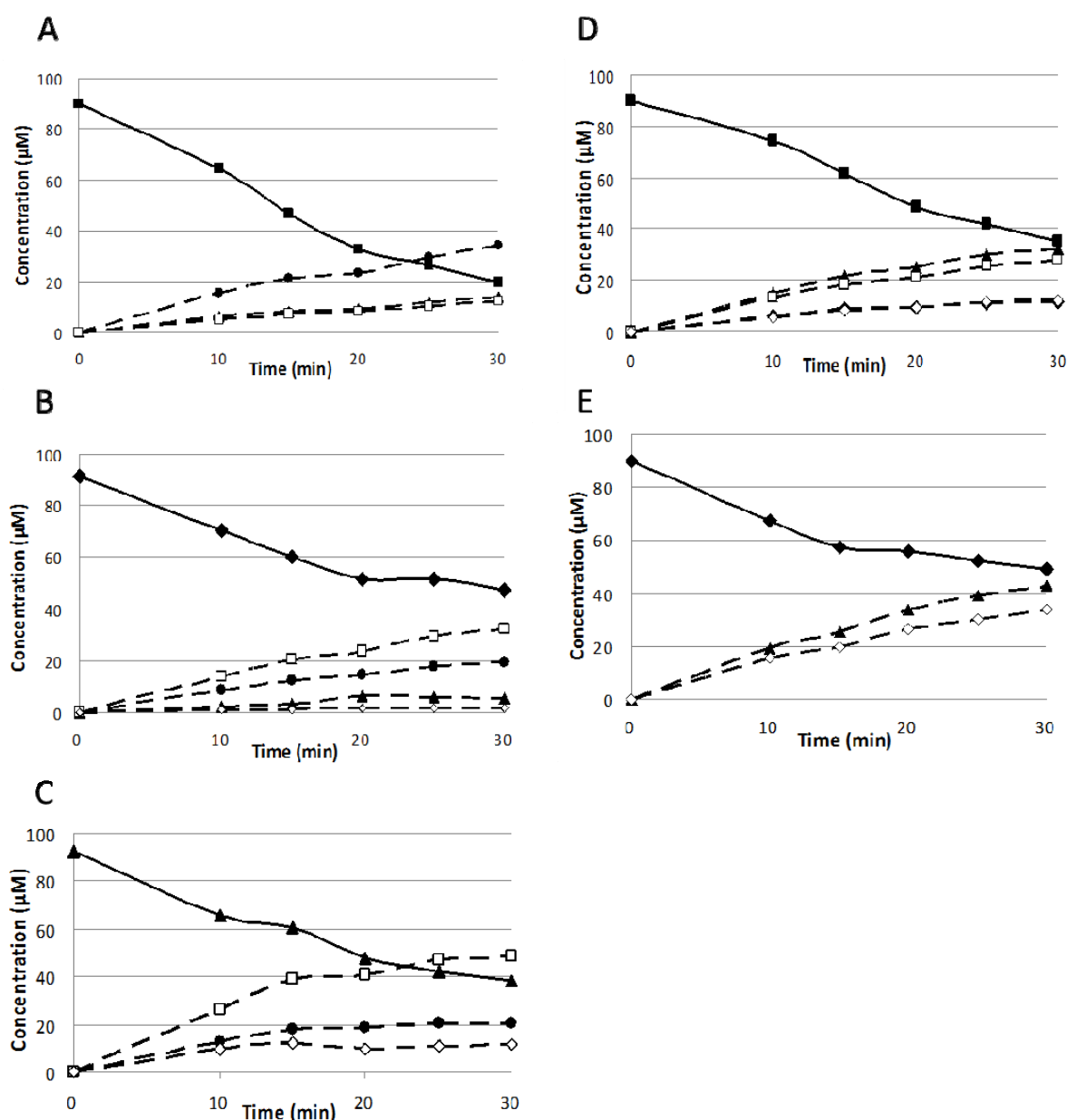


Figure 2

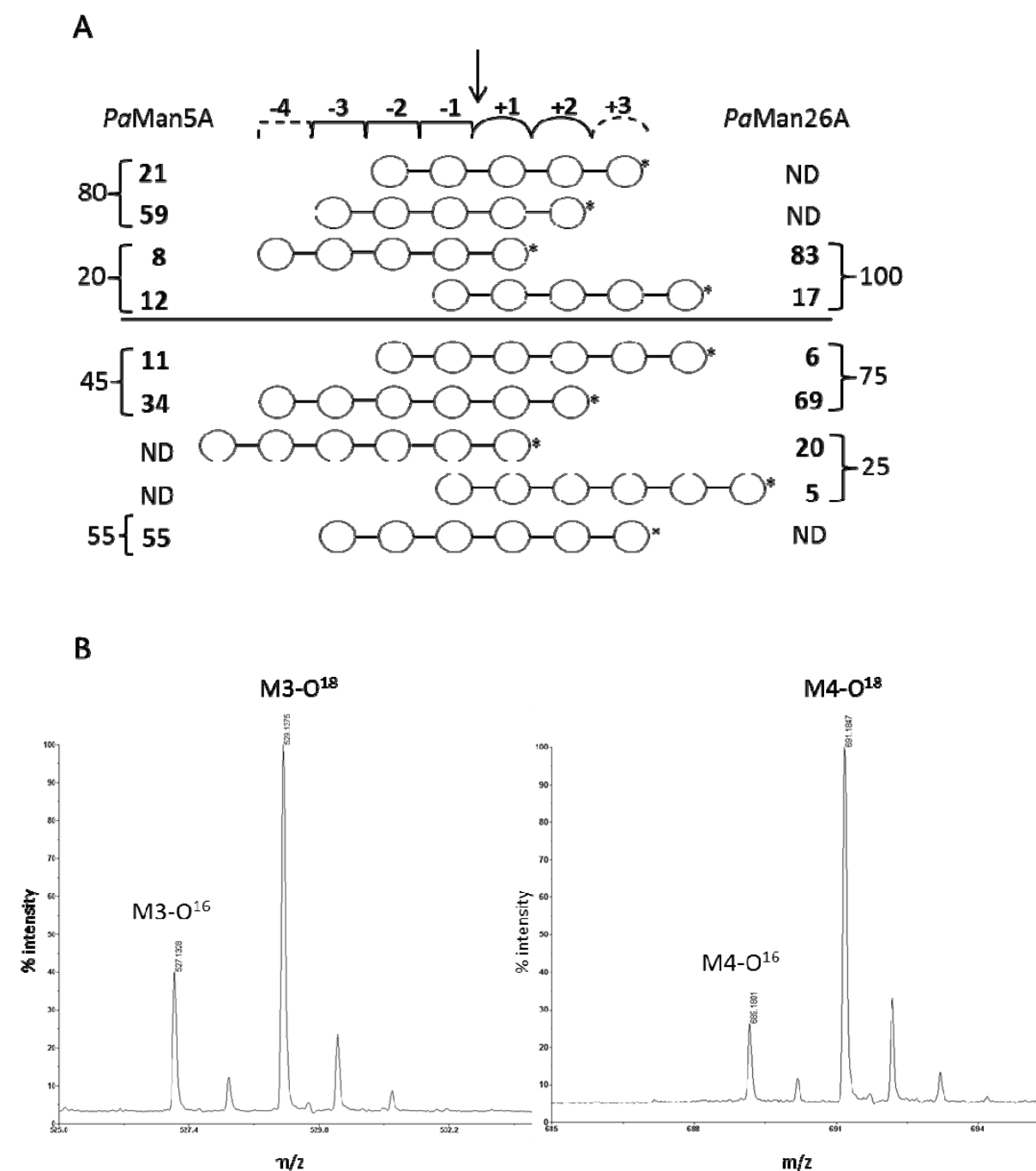


Figure 3

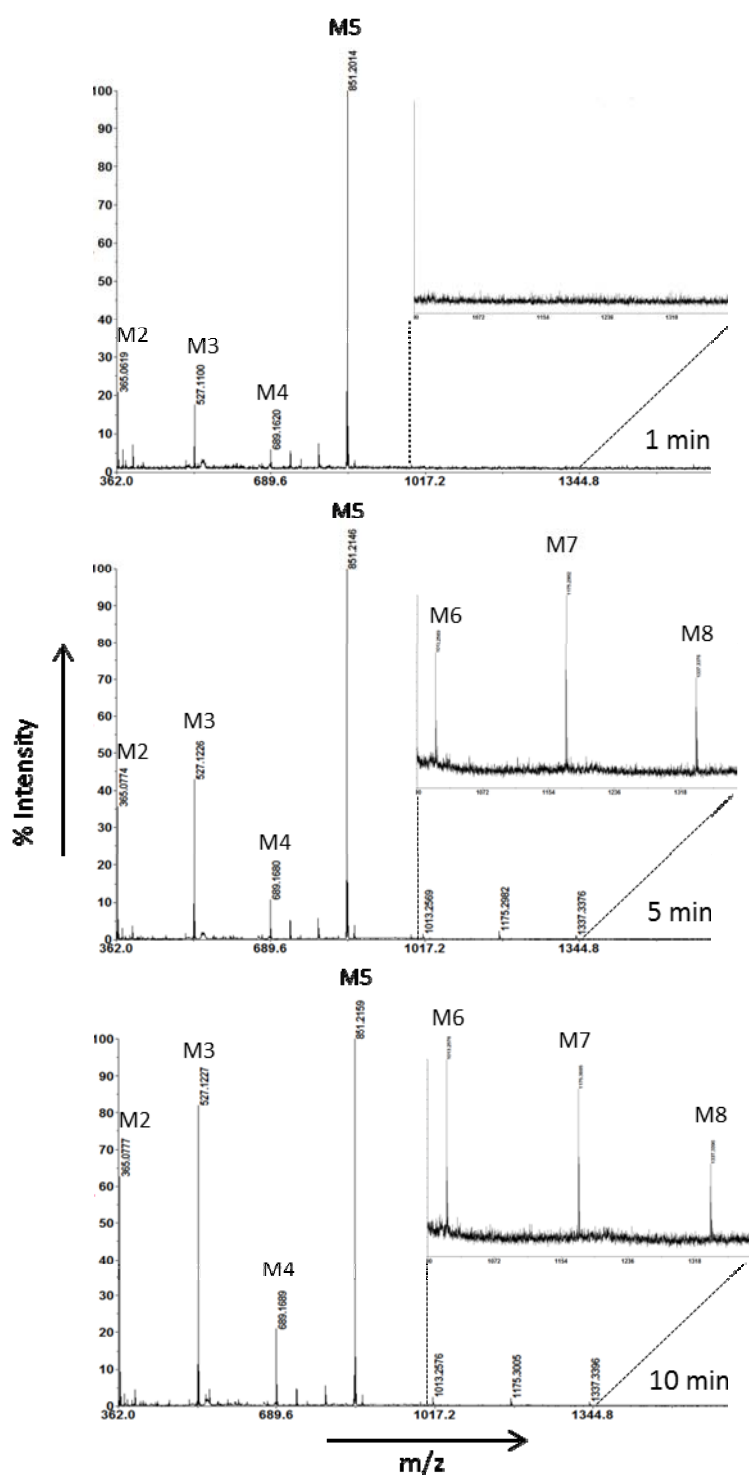


Figure 4

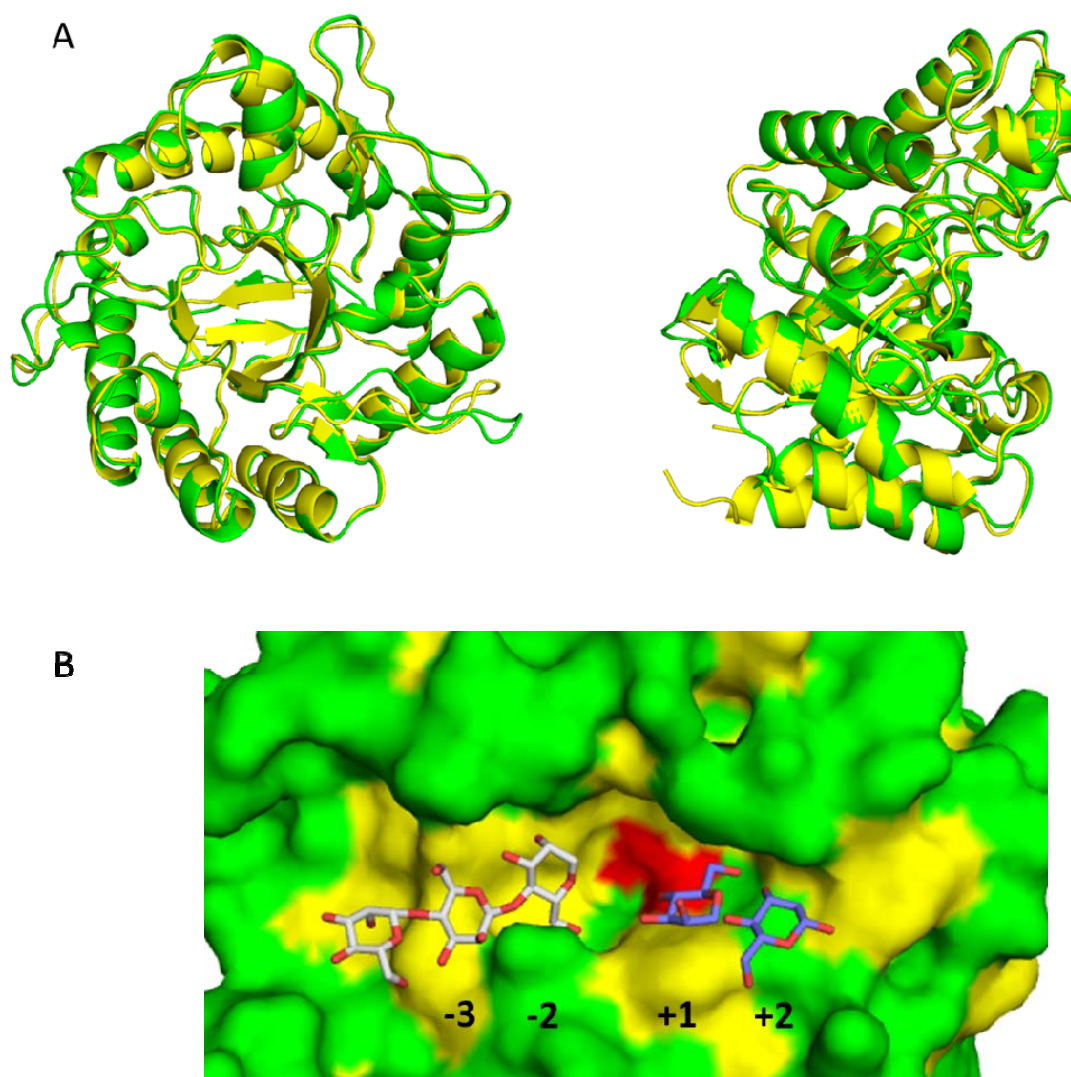


Figure 5

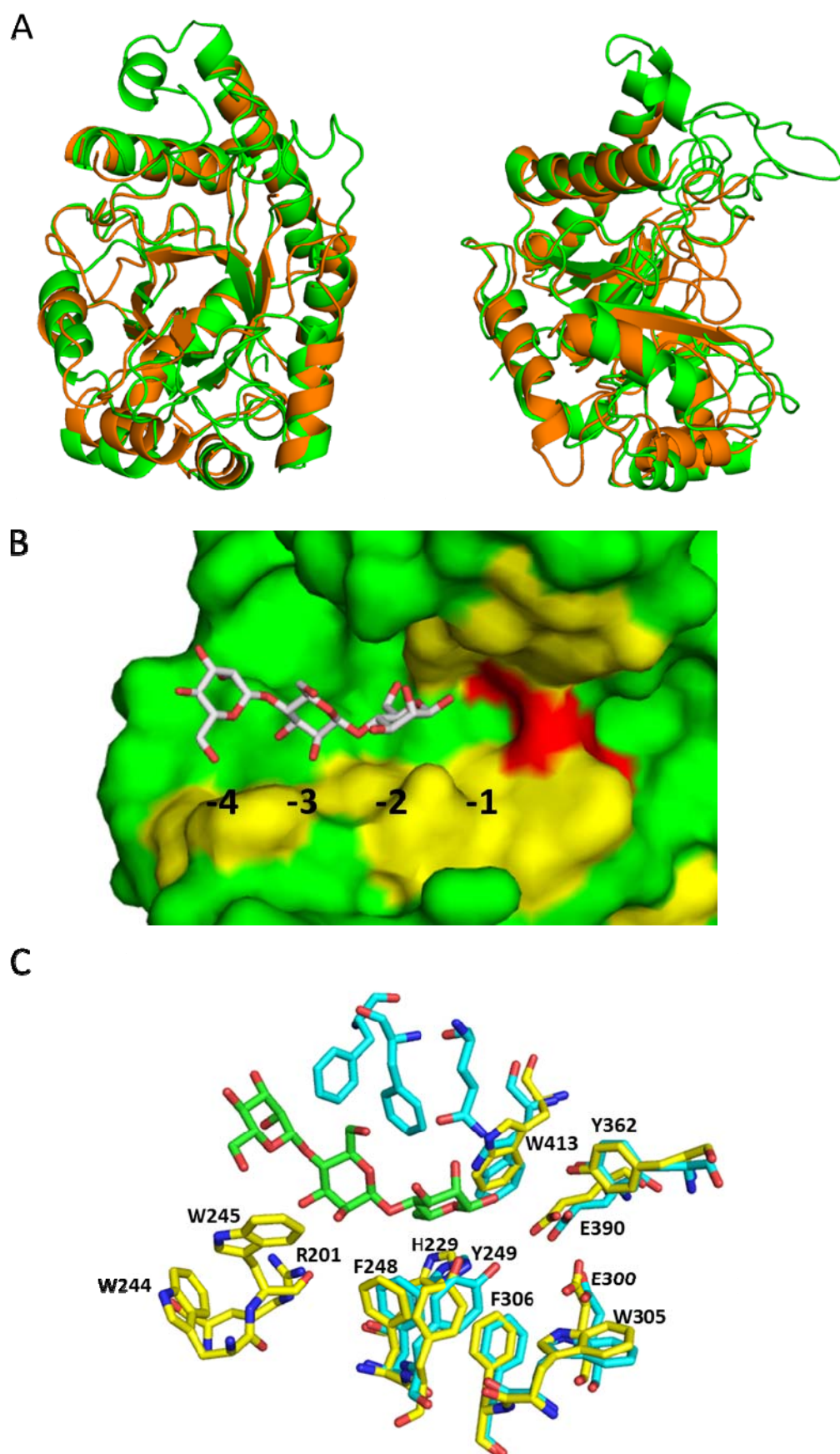


Figure 6

